CALIBRATION OF THE OSCILLATING SCREEN VISCOMETER

Robert F. Berg and Michael R. Moldover
Thermophysics Division
National Institute of Standards and Technology

[29 October 1993]

Summary

We have devised a calibration procedure for the oscillating screen viscometer which can provide the accuracy needed for the flight measurement of viscosity near the liquid–vapor critical point of xenon. The procedure, which makes use of the viscometer's wide bandwidth and hydrodynamic similarity, allows the viscometer to be self–calibrating. To demonstrate the validity of this procedure we measured the oscillator's transfer function under a wide variety of conditions. We obtained data using CO_2 at temperatures spanning a temperature range of 35 K and densities varying by a factor of 165, thereby encountering viscosity variations as great as 50%. In contrast the flight experiment will be performed over a temperature range of 29 K and at only a single density, and the viscosity is expected to change by less than 40%.

The measurements show that, after excluding data above 10 Hz (where frequency–dependent corrections are poorly modeled) and making a plausible adjustment to the viscosity value used at high density, the viscometer's behavior is fully consistent with the use of hydrodynamic similarity for calibration. Achieving this agreement required understanding a 1% anelastic effect present in the oscillator's torsion fiber.

1. Introduction

Of the several goals of the Critical Viscosity Experiment, the most easily quantifiable is determination of the exponent for the divergence of viscosity near the liquid–vapor critical point. In order to meet the nominal goal of determining this exponent to within ±1% without reliance on the details of an accurate crossover theory, the measured viscosity must be proportional to the true viscosity to within ±0.2% [1]. Achieving this requires accurate knowledge of three aspects of the experiment. These are the viscometer's hydrodynamics, all nonviscous forces, and instrumental effects such as amplifier nonlinearity.

Because measurement of viscosity to an absolute accuracy of ±0.2% is difficult, it is rarely achieved. Fortunately, in order to test the theory for the viscosity divergence, it is unimportant if the measured viscosity differs from the true viscosity by an arbitrary scale factor. To quantify the effects of other errors, suppose that the measured viscosity η_m is a quadratic function of the true viscosity η, namely

$$\eta_m = a_0\eta_1 + a_1\eta + (a_2/\eta_1)\eta^2 , \qquad (1)$$

where η_1 is a reference viscosity far from T_c. The important error is the deviation from proportionality. For small errors, this quantity can be written as

$$\frac{\eta_{m2}/\eta_{m1}}{\eta_2/\eta_1} - 1 \cong -\left[\frac{a_0}{a_1}\right]\left[\frac{\eta_2-\eta_1}{\eta_2}\right] + \left[\frac{a_2}{a_1}\right]\left[\frac{\eta_2-\eta_1}{\eta_1}\right] . \qquad (2)$$

The suffix 2 refers to the reduced temperature 2×10^{-6}. If the reference viscosity is at the reduced temperature 2×10^{-4}, then the change of viscosity anticipated in the flight experiment is approximately

$$\eta_2 - \eta_1 \cong 1.2\ \eta_1 . \qquad (3)$$

In Eq.(2), the value of a_1 need not be known; rather the sum of the first term, or "zero offset", and the second term, or "nonlinearity", must be less than 0.2%.

The hydrodynamic theory for most viscometers starts with an ideal geometry, for example a cylinder. Corrections for nonideal features such as edges or ellipticity are almost always required, and they are either calculated with an elaboration of the hydrodynamic model or measured in ancillary experiments. These corrections must be known throughout the ranges of frequency, density, and viscosity in which the viscometer operates. For the oscillating screen viscometer, the ideal geometry is the transversely oscillating cylinder. The most important correction to this model is the use of an effective cylinder radius chosen to best match the oscillator's behavior. To achieve the needed accuracy by this route, further corrections, determined by experiments with calibrating fluids and possibly of an ad hoc form, would be needed.

However, there is another, more powerful method to accurately characterize the hydrodynamics of the oscillating screen viscometer, made possible by the fact that the viscometer is sensitive to viscosity over a relatively wide frequency bandwidth. As explained in Section 2 on hydrodynamic similarity, this method does not rely on a specific hydrodynamic model, and it allows the viscometer to be self–calibrating.

The calibration tests described in Section 3 verified the applicability of hydrodynamic similarity for measuring changes in the viscosity with the oscillating screen. Our measurements of viscosity changes were consistent with the best viscosity measurements available in the literature ("±0.1%"). We note that, because we were comparing changes of the viscosity, the accuracy of this comparison was ±1% at best, worse than the required ±0.2%. However, the consistency achieved in a wide range of conditions described in Section 3 gives us confidence that the instrument has the necessary accuracy for use in the Critical Viscosity Experiment.

Section 4 outlines a calibration procedure based hydrodynamic similarity.

2. Hydrodynamic similarity

An torsion oscillator can be characterized by measurements of its transfer function $H(\omega)$, defined by

$$H(\omega) \equiv \frac{\theta(\omega)}{\tau(\omega)}, \tag{4}$$

where $\theta(\omega)$ and $\tau(\omega)$ are the measured angular displacement and $\tau(\omega)$ is the applied torque. (At present we can measure only the product $k_{tr}H$, where k_{tr} is an inaccurately known transducer coefficient assumed to be independent of frequency.) By immersing it in a fluid, an oscillator can be used as a viscometer, but only over a finite frequency bandwidth. This bandwidth can be defined as the frequency range where the viscometer's sensitivity, defined by the dimensionless quantity

$$\frac{\eta}{H}\frac{\partial H}{\partial \eta}, \tag{5}$$

is comparable to unity. (Fig. 1 shows examples.) For high–Q oscillators the sensitivity is significant only in a narrow frequency range near the vacuum resonance frequency ω_0. In contrast, for a low–Q oscillator such as the oscillating screen viscometer, viscosity can be measured over a broad frequency range. Equivalently, at a fixed density ρ and viscosity η, the viscometer is sensitive to viscosity over a broad range of viscous penetration lengths δ, defined by

$$\delta \equiv \left[\frac{2\eta}{\rho\omega}\right]^{1/2}. \tag{6}$$

Although hydrodynamic similarity most often refers to scaling of the Navier–Stokes equation with the Reynolds number, here we are interested in the similarity that exists for small amplitude oscillatory flow. The linear Navier–Stokes equation can then be written in terms of a dimensionless velocity, pressure, time, and spatial derivative, u', p', t', and ∇' by rescaling their dimensional equivalents with respect to a characteristic length R, a characteristic time ω^{-1}, and a characteristic pressure $\eta\omega$. The result,

$$\frac{\partial u'}{\partial t'} = \frac{\eta}{\rho\omega R^2}\nabla p' + \frac{\eta}{\rho\omega R^2}\nabla'^2 u' , \qquad (7)$$

is an equation parameterized only by the ratio $(\delta/R)^2$.

This result can be combined with the harmonic oscillator equation to give the oscillator's response function $H(\omega)$ in terms of the dimensionless frequency $\Omega \equiv \omega/\omega_0$:

$$H(\omega)^{-1} = k_\theta[(1-\Omega^2) + i\Omega^2(\rho/\rho_s)B(R/\delta)] . \qquad (8)$$

Here, ρ and ρ_s are the densities of the fluid and the oscillator body respectively, k_θ is the oscillator's spring constant, and $B(R/\delta)$ is a function characteristic of the oscillator's geometry. (The convention $e^{+i\omega t}$ is used.) The most important feature of Eq.(8) is that the oscillator's transfer function depends on the fluid's viscosity only through the viscous penetration length.

Eq.(8) requires that the oscillator be characterized by only the undamped resonance frequency ω_0, the oscillator's density ρ_s, and the spring constant, $k_\theta = I\omega_0^2$, where I is the oscillator's moment of inertia. The frequency ω_0 can be accurately measured in vacuum. The value chosen for the oscillator's density ρ_s is unimportant because it divides the function $B(R/\delta)$. In effect the product $(\rho/\rho_s)B$ is measured in the calibration. For the oscillating screen, we estimated ρ_s by weighing a representative piece of the screen and then modeling the screen as a single cylinder of radius R. The geometry of the oscillator's torsion fiber was too complex to calculate the spring constant k_θ to the needed accuracy. However, the ratio k_{tr}/k_θ, where k_{tr} is the transducer coefficient, could be obtained directly by measuring the response function $H(\omega)$ in the limit of 0 Hz. This required an understanding of the torsion fiber's anelasticity, described in Appendix C.

The function $B(R/\delta)$ is known exactly only for simple geometries. For an arbitrarily complicated geometry, it can be inferred from measurements of the oscillator's transfer function.

$$B(R/\delta) = \frac{[(k_\theta/k_{tr})H(\omega)]^{-1} - (1-\Omega^2)}{i\Omega^2(\rho/\rho_s)} . \qquad (9)$$

For an imperfectly known geometry, the dependence of B on the viscous penetration length

δ can be obtained by either (1) the use of a single frequency with various calibrating fluids or by (2) the use of a single calibrating fluid measured at various frequencies. The first strategy is limited by the accuracy of the calibrating fluids' viscosities. (Density inaccuracy is assumed to be insignificant.) In contrast, because the second strategy makes use of only one fluid, it is potentially highly accurate for calibrating a viscometer intended to measure relative changes, as is the case for the planned Critical Viscosity Experiment. The second strategy can be implemented only in a wide–bandwidth viscometer, also true for the planned flight experiment. Appendices A and B explain in more detail the necessity of using a low–Q oscillator to achieve a wide bandwidth in the viscosity measurement.

Calibration of the oscillating screen viscometer amounts to a measurement of the hydrodynamic geometry function $B(R/\delta)$ over a range of viscous penetration lengths encompassing the intended operating conditions. This can be done with any fluid having a kinematic viscosity similar to xenon. Furthermore, for the measurement of relative viscosity changes, the viscometer is self–calibrating, namely no fluid other than xenon will be needed.

Self–calibration is possible because the anticipated variation of δ caused by changing the temperature is less than the variation of δ induced by changing the frequency at a single temperature. For example, for the flight experiment in xenon close to T_c, δ at 5 Hz is expected to be no more than 20% greater than the minimum far from T_c. The same penetration length can be obtained far from T_c at 3.5 Hz, which, as indicated by Fig. 1, is within the bandwidth of the viscometer.

3. Tests of the applicability of hydrodynamic similarity

A. Choice of fluid

Carbon dioxide was chosen as the calibrating fluid because accurate viscosity data for CO_2 are available at kinematic viscosities comparable to that of xenon at its critical density. This criterion excluded liquids such as water and toluene. The additional requirement of operation between 0 and 60° C and at pressures less than 10 MPa excluded other well–measured gases such as argon and nitrogen. We excluded SF_6 because its viscosity is known less accurately than that of CO_2.

We made use of previous viscosity measurements included in the recent correlation of Vesovic et al. [2]. We initially considered the use of four density ranges: low (where $\partial\eta/\partial\rho$ is small), moderate but below the critical region, the critical region, and above the critical region. The most accurate measurements were made at low densities near room temperature. For these data we used the representation of Kestin, Ro, and Wakeham [3].

Within ±0.2%, the data from Kestin's group agree with both the more recent measurements by Vogel and Barkow [4] and the correlation of Ref.[2] over the 25–61° C temperature range used in the present measurements.

At moderate densities we again used measurements from Kestin's group. Kestin, Korfali, and Sengers [5] reported viscosity measurements made at 31.6 °C and at densities up to 307 $kg \cdot m^{-3}$. At the higher densities, their values disagree by as much as 1% with the older measurements of Kestin, Whitelaw, and Zien [6]. This latter set we found useful because it reported the temperature dependence at moderate densities.

We used no measurements made at densities near the critical density of CO_2. Vesovic et al. state that for densities ρ outside the limits $300\ kg \cdot m^{-3} < \rho < 600\ kg \cdot^{-3}$, the critical viscosity enhancement is less than 1%. Inside this region, experimental difficulties are greater, and Vesovic et al. could not correlate the data of Iwasaki and Takahashi [7] to better than 2%. Our own measurements [8] close to the critical point of CO_2 were made only at the critical density.

We made no measurements above 600 $kg \cdot m^{-3}$ because of the high pressures involved.

The kinematic viscosity of CO_2 is always higher than that of xenon at critical density. (The minimum kinematic viscosity tends to occur near the critical density.) This is not surprising: with the usual exceptions of ^3He and ^4He, xenon's high molecular weight causes its minimum kinematic viscosity to be less than that of any other fluid. However, the necessary range of penetration depths could still be covered by our CO_2 measurements. In the flight experiment, the expected range for the penetration length in xenon at 5 Hz is

$$55\ \mu m < \delta < 66\ \mu m \quad [10^{-2} < (T-T_c)/T_c < 10^{-7}]. \tag{10}$$

This range of penetration lengths was easily spanned by the present measurements. For example, this was done with CO_2 at 295 $kg \cdot m^{-3}$ by operating the viscometer between 5.6 and 8.1 Hz.

B. Technique

In principle self–calibration need be done only after the viscometer is loaded with xenon; the present tests were made to demonstrate the applicability of hydrodynamic similarity for the oscillating viscometer. Potential causes of failure included all three aspects mentioned in the Introduction's first paragraph. For example, the flow could have been too large for the linearized Navier–Stokes equation to apply, there could have been an

unexpected coupling to a bending mode of the screen, or the transducers could have had an unexpected frequency dependence. To look for such effects, we covered a wide range of conditions. We spanned a factor of 165 in density and a 50% change in both the viscosity and the kinematic viscosity. Measurements were made up to 25 Hz in the temperature range from 25 to 61°C. In contrast, the flight experiment will take place in a narrow range of conditions. Only one density will be used, and the viscosity is expected to change by less than a 40%. Frequencies less than 12.5 Hz will be used in the narrower temperature range of 16 to 45°C.

Using the method previously described [1], we measured the oscillator's transfer function over the range 0–25 Hz at the five densities and temperatures listed in Table 2. The densities, determined by weighing the filled cell, were chosen to fall near those used Kestin, Whitelaw, and Zien [6]. We also made measurements at low frequencies to obtain the transducer coefficient k_{tr}. Preceding these tests, we made measurements of the oscillator's resonance frequency and Q in vacuum between 7 and 81°C. In many cases, we extended the measurement time to several hours to improve the signal–to–noise ratio. In most of the data plots, the trends of the data are clarified by averaging the data in groups of 10.

C. Density dependence of η near room temperature

Fig. 2 shows the frequency response measured at four of the five different densities. (The data at 242.8 $kg \cdot m^{-3}$ are similar to those at 295.1 $kg \cdot m^{-3}$ and are omitted for clarity.) The viscometer was sensitive to viscosity changes over most of the measured frequency range. This is indicated by Fig. 1, which shows the viscometer's sensitivity when modeled as an ideal cylinder oscillating in CO_2 at a density of 295.1 $kg \cdot m^{-3}$. For example, at 8 Hz, a viscosity change of 10% would change the oscillator's response by about 8%.

Using Eq.(9), we derived values of the function $B(R/\delta)$. The results, which include corrections for the spring's anelastic character (Appendix C) and the effects of four low–pass electronic filters (Appendix D), are shown in Fig. 3. Also plotted is the value of $B_c(R/\delta)$ calculated for the case of a transversely oscillating cylinder of radius R≡13.8 μm [9]. (For clarity, $(R/\delta)^2|B|$, not $|B|$, is plotted.)

The consistency of the data can be examined more closely in Fig. 4, which is a plot of the ratio $|B/B_c|$. To the extent that the data fall on a single, smooth curve, they are consistent with the expected hydrodynamic similarity. However, there are two types of

small discrepancies. The first kind occurs at higher frequencies, especially above 15 Hz. An example is the upturn near R/δ=0.04 of the data taken at 1.79 $kg \cdot m^{-3}$. This discrepancy may be due to incorrect modeling of the corrections for anelasticity or of the electronic filters. For example, in modeling the effect of a low–pass filter on the output of the square root amplifier we ignored the frequencies of all but the fundamental Fourier component. Also, we made no attempt to characterize anelastic effects above the resonance frequency of $\omega_0/2\pi = 11.5$ Hz.

The second kind of discrepancy, which occurs between the data at 295.1 and 90.1 $kg \cdot m^{-3}$, can be removed if the value of the viscosity used at the higher density is reduced by 1%. This adjustment can be partially justified in two ways. First, as shown in Fig. 5, it yields a curve with continuous slope as well as value. Second, the amplitude of the adjustment is consistent with both the scatter of the original data and with the disagreement between the values of Kestin, Korfali, and Sengers [5] and of Kestin, Whitelaw, and Zien [6]. The viscosity data of Ref. [6] are about 1% less than those of Ref. [5] near 300 $kg \cdot m^{-3}$.

Fig. 5 shows the experimentally derived function $B(R/\delta)$ after addressing both discrepancies. Only data between 1 and 10 Hz were used, and the value of the viscosity used at 295.1 $kg \cdot m^{-3}$ from Kestin, Korfali, and Sengers [5] was lowered by 1%. The result is a smoothly varying function of penetration length that is independent of density and is fully consistent with hydrodynamic similarity. The strongest deviations from the cylinder model occur at large viscous penetration lengths, or low values of R/δ. This is to be expected for $R/\delta < 0.033$, where δ is half the distance between screen wires. We emphasize that the cylinder model was used only as a convenience to examine the data. No explicit hydrodynamic model is needed to obtain the hydrodynamic geometry function $B(R/\delta)$. Also, the value chosen for the characteristic length R is unimportant for the calibration as long as the same length is used for both calibration and measurement.

D. Temperature dependence of η at moderate density

Fig. 6 shows plots of $|B/B_c|$ as a function of R/δ obtained at 31.6, 34.6, and 40.6° C for a constant density of 242.8 $kg \cdot m^{-3}$. For consistency in this comparison we used only data from one investigation, that of Kestin, Whitelaw, and Zien [6]. Over the range $0.2 < R/\delta < 0.3$ the data for $|B/B_c|$ obtained at 31.6 and 40.6° C are consistent to within ±0.1% of the viscosity. The viscosity changes by 2.9% between these two temperatures.

Although noisier, the data at 34.6° C are significantly higher over the same range in R/δ, corresponding to a viscosity disagreement of as much as –0.2%. We do not know the source of this small disagreement.

E. Temperature dependence of η at low density

We measured the oscillator's transfer function in CO_2 at 25.6, 40.6, and 60.6° C for a constant density of 1.79 $kg \cdot m^{-3}$. Fig. 7 shows the transfer function measured at the three temperatures. (The temperature accuracy is ±0.1 K.)

Although, the resulting variation in the viscosity (11%) was less than that resulting from varying the density, these tests were important for two reasons. First, the most accurate data for the viscosity are at low density. Second, the flight experiment will measure viscosity variation vs. temperature and thus is susceptible to systematic errors caused by temperature changes. To avoid exceeding the cell's pressure tolerance, the temperature range required to look for such errors is best explored at low density.

The consistency of the values derived for the hydrodynamic geometry function $B(R/\delta)$ can be seen in Fig. 8. As previously noted, there are small unexplained discrepancies at higher frequencies. However, the agreement is excellent up to about R/δ=0.028 or about 12 Hz. In this frequency range, the corresponding discrepancies in viscosity fall within ±0.1%. This error $\Delta\eta$ is consistent with the data of Kestin, Ro, and Wakeham [3] within their stated accuracy. Although, this comparison does not test the viscometer's ability to measure absolute viscosity, it does test the viscometer's ability to measure the variation of viscosity with temperature. The agreement in the latter quantity is

$$\frac{\Delta\eta}{\eta(60.6^\circ C) - \eta(25.6^\circ C)} = \frac{\pm 0.1\,\%}{\pm 11\%} = \pm 1\% \,. \qquad (11)$$

Thus, the oscillating's screen performance is consistent with the most accurate viscosity data available.

4. Calibration procedure

The following procedure will be used for the flight experiment.

(1) With the viscometer cell evacuated, measure the oscillator's transfer function between 0.001 Hz and the resonance frequency (about 11.5 Hz) at temperatures between 10 and 60° C. This will determine the anelastic corrections to the torsion

fiber's spring constant.

(2) With the viscometer cell evacuated, measure the transfer function near the resonance frequency at temperatures between 10 and 60° C. This will determine the temperature dependence of the oscillator's resonance frequency ω_0 and quality factor Q.

(3) After the loading the viscometer cell with xenon at its critical density, measure the transfer function between 1 and 12.5 Hz at a temperature T_{cal} sufficiently far from T_c to eliminate significant effects due to stratification in Earth's gravity (say $T_{cal} = T_c + 3$ K). This will determine the hydrodynamic geometry function $B_{cal}(\delta)$ over the range of δ expected at 5 Hz in the flight experiment. This measurement will also be done during the flight experiment, in effect calibrating the viscometer in orbit.

(4) Viscosity values at T close to T_c will be obtained by
(a) Measuring $H(\omega)$ at the temperature T.
(b) Using Eq.(9) to obtain B(T).
(c) Using $B_{cal}(\delta)$ to invert B(T) and thereby obtain δ.
(d) Calculating $\eta = (1/2)\rho\omega\delta^2$.

The resulting viscosity values will be relative to the viscosity at the calibrating temperature T_{cal}. This has already been measured to an accuracy of 0.8% [8].

Appendix A: Bandwidth of an oscillator viscometer

The oscillating screen viscometer's calibration relies on viscosity measurements made over a substantial range of frequencies. This section explains why, for fixed spring constant, an overdamped, or "low–Q" oscillator is necessary for such measurements.

Low–Q oscillators are superior for measuring viscosity over a wide range of frequencies because the transfer function of a high–Q oscillator is sensitive to dissipation only near its resonance frequency ω_0. This can be illustrated by considering a torsion oscillator with moment of inertia I, spring constant k_θ and frequency–independent dissipation coefficient ν. For a sinusoidal torque $\tau(\omega)$ of fixed amplitude, the angular displacement θ is given by

$$\theta = \frac{\tau(\omega)}{[-I\omega^2 + i\omega\nu + k_\theta]}. \tag{A1}$$

Changes in ν can be detected through changes in θ. The oscillator's sensitivity to dissipation is measured by the normalized derivative

$$\frac{\nu}{\theta}\frac{\partial\theta}{\partial\nu} = \frac{-i\omega\nu}{[-I\omega^2 + i\omega\nu + k_\theta]}. \tag{A2}$$

Making the substitutions

$$k_\theta = I\omega_0^2 \tag{A3}$$

and

$$Q \equiv \frac{I\omega_0}{\nu} \tag{A4}$$

allows the oscillator's sensitivity to dissipation to be rewritten as

$$\frac{\nu}{\theta}\frac{\partial\theta}{\partial\nu} = \frac{-i\,\Omega}{[1-\Omega^2]Q + i\Omega}, \tag{A5}$$

where $\Omega \equiv \omega/\omega_0$ is the reduced frequency. (The definition of Q in Eq.(A4) is the usual quality factor generalized to include overdamped oscillators.)

Eq.(A5) shows that an oscillator's amplitude is most sensitive to changes of the dissipation coefficient at resonance. Far below resonance the elastic restoring force is much greater than the dissipative force, and far above resonance inertia is dominant. The oscillator's Q determines what is "near" and what is "far". Table 3 illustrates this point by using Eq.(A5) to compare the magnitudes of the dissipation sensitivities of two hypothetical oscillators whose Q's differ by a factor of 100. For example, if the oscillator with Q=10 is driven with constant torque at half its resonance frequency, a 100% increase in the dissipation will cause only a 6.7% decrease in the oscillator's amplitude.

The bandwidth in which the oscillator is sensitive to dissipation can be defined by the lower and upper frequencies ω_- and ω_+ where the magnitude of the sensitivity falls to 1/2. The relation of this bandwidth to the Q is given by

$$\frac{\omega_+ - \omega_-}{\omega_0} = \frac{\sqrt{3}}{Q}. \tag{A6}$$

For a highly damped oscillator ($Q<<1$) the bandwidth is more appropriately characterized by the ratio

$$\frac{\omega_+}{\omega_-} \cong \frac{3}{Q^2}. \tag{A7}$$

In contrast to the preceding illustration, the dissipation coefficient ν of an oscillator viscometer is a complex function of frequency. Although this complicates the analysis, numerical calculations with specific hydrodynamic models [10] show that the above result

still holds qualitatively, namely a low–Q oscillator is sensitive to changes in the viscosity over a wider range of frequencies than a high–Q oscillator.

The signal–to–noise ratio of a viscometer is determined both by its sensitivity to dissipation and by noise in the measurement. Thus, if a viscometer is operated outside its bandwidth, its insensitivity to the viscosity can be at least partially compensated by reducing the accompanying noise. This issue is quantified in Appendix B.

Appendix B: Signal–to–noise ratio of an oscillator viscometer

The oscillating screen viscometer was developed because the Space Shuttle's typical vibration environment was predicted to degrade the precision of our earlier, high–Q oscillator technique to an unacceptable level. The advantage of a low–Q oscillator can be understood qualitatively by recalling that the rms noise magnitude of a high–Q oscillator at resonance is proportional to the oscillator's Q. In contrast, as shown by Eq.(A5), its sensitivity to changes in the dissipation is independent of Q. Thus, high–Q viscometers suffer more from random vibration. In the following, this argument is refined through a derivation of the signal–to–noise ratio for a measurement of an oscillator's dissipation.

First, we will consider the detrimental effect of mechanical vibrations on the signal–to–noise ratio. Our model is an oscillator whose spring is attached to a randomly vibrating wall. When the oscillator is driven by changes of the wall's angular position θ_w, the equation of motion is

$$I\frac{d^2\theta}{dt^2} + \nu\frac{d\theta}{dt} + k_\theta(\theta - \theta_w) = 0 \qquad \text{(B1)}$$

Because the position–sensing electrodes are fixed to the wall, we are interested in the root–mean–square difference of the oscillator's position with respect to the wall's position, namely

$$\delta\theta \equiv [<(\theta - \theta_w)^2>]^{1/2} . \qquad \text{(B2)}$$

The transfer function derived from Eq.(B1) then gives the rms magnitude of the oscillator's position $\delta\theta$ as a function of the rms magnitude of the wall's position $\delta\theta_w$ as

$$\delta\theta = \frac{[1 + (Q\Omega)^2]^{1/2}}{[(1-\Omega^2)^2 Q^2 + \Omega^2]^{1/2}}\,\Omega\,\delta\theta_w . \qquad \text{(B3)}$$

Eq.(B3) gives the "noise" in the oscillator's signal–to–noise ratio. The "signal" is defined as the change $\Delta\theta_0$ in the oscillator's amplitude θ_0 caused by a change $\Delta\nu$ in the oscillator's dissipation, namely

$$\Delta\theta_0 = \left|\frac{\nu}{\theta}\frac{\partial\theta}{\partial\nu}\right|\frac{\Delta\nu}{\nu}\,\theta_0 . \qquad \text{(B4)}$$

Using Eq.(A5) this is

$$\Delta\theta_0 = \frac{\Omega}{[(1-\Omega^2)^2Q^2 + \Omega^2]^{1/2}} \frac{\Delta\nu}{\nu}\,\theta_0 . \qquad \text{(B5)}$$

(Information contained in changes of the oscillator's phase are ignored here. This does not change the overall conclusions.) The ratio of Eqs.(B3) and (B5) gives the signal–to–noise ratio as

$$\frac{\Delta\theta_0}{\delta\theta_w} = [1 + (Q\Omega)^2]^{-1/2} \frac{\theta_0}{\delta\theta_w} \frac{\Delta\nu}{\nu} . \qquad \text{(B6)}$$

Eq.(B6) says that the signal–to–noise ratio of a dissipation measurement degrades significantly when the oscillator is operated at a reduced frequency $\Omega > Q^{-1}$.

Eq.(B6) also says that the signal–to–noise ratio is independent of Q in the limit of low reduced frequency. This unrealistic result occurred because sources of noise besides vibration were ignored. For example, usually there is also an electronic noise source of magnitude $\delta\theta_e$ which, unlike $\delta\theta$, depends only weakly on frequency. Including such noise in the signal–to–noise ratio gives

$$\frac{\Delta\theta_0}{[\delta\theta^2+\delta\theta_e^2]^{1/2}} = \frac{\theta_0}{\{[1+Q^2\Omega^2]\delta\theta_w^2 + [1+Q^2(\Omega-1/\Omega)^2]\delta\theta_e^2\}^{1/2}} \frac{\Delta\nu}{\nu} . \qquad \text{(B7)}$$

Examination of Eq.(B7) reveals several ways to improve the signal–to–noise ratio. Perhaps the most obvious is to increase the amplitude θ_0. There are two limits on this strategy. First, the fluid itself has a limiting nonlinearity near the critical point. The oscillating screen viscometer is normally operated near the shear rate S characteristic of xenon at a reduced temperature of $\epsilon=2\times10^{-6}$. The associated amplitude is

$$\theta_0 = \frac{S\delta}{L\omega} \approx 10^{-3} \text{ radian}, \qquad \text{(B8)}$$

where δ is the viscous penetration length and L ≈ 0.01 m is the radius of the screen. Due to the scaling of the oscillator's resonance frequency with size, the operating frequency ω cannot be reduced much from its nominal value of 5 Hz. Second, due to the finite dynamic range of any electronic system, the ratio $\delta\theta_e/\theta_0$ cannot be reduced indefinitely by increasing θ_0.

As expected from the earlier qualitative argument, Eq.(B7) says that the signal–to–noise ratio can be improved by decreasing the oscillator's Q. An exception occurs for operation at resonance with dominant electronic noise, namely $\delta\theta_e/\delta\theta_w >> Q$. The signal–to–noise ratio is then

$$\frac{\Delta\theta_0}{[\delta\theta^2+\delta\theta_e^2]^{1/2}} \cong \frac{\theta_0}{\delta\theta_e} \frac{\Delta\nu}{\nu} , \qquad \text{(B9)}$$

which is independent of Q. Eq.(B9) is more likely to apply at higher frequencies due to

suppression of the vibration noise magnitude $\delta\theta_w$.

A further improvement is to operate at the frequency where the denominator of Eq.(B7) is smallest. Assuming the noise drivers $\delta\theta_w$ and $\delta\theta_e$ are frequency–independent, this optimum frequency is

$$\Omega = \left[\frac{\delta\theta_e^2}{\delta\theta_w^2 + \delta\theta_e^2}\right]^{1/4} . \qquad \text{(B10)}$$

Because Eq.(B10) is independent of Q, the optimum frequency can fall below even the oscillator's bandwidth of sensitivity to dissipation.

Finally, the signal–to–noise ratio can be improved by using vibration isolation to reduce $\delta\theta_w$, by using low–noise electronics to reduce $\delta\theta_e$, and by increasing the measuring time.

In addition to bandwidth and vibration insensitivity, there are two additional considerations for comparing low–Q and high–Q viscometers. The first consideration is that a higher–frequency mode of the oscillator can contribute to the transfer function and thereby complicate its analysis. This problem is more likely if the extra mode is nearby in frequency and, like the primary mode, has a low Q. Presumably, an analysis based on hydrodynamic similarity and additional calibration measurements could still be applied in this situation. Instead we used a simpler approach. First, we designed the oscillator so that the frequency of the next lowest mode was 5 times higher than ω_0. Second, we verified the consistency of results obtained at the same penetration length but with differing combinations of viscosity, density, and frequency. The extra effort needed to eliminate problems caused by higher modes is a disadvantage of low–Q oscillators.

The second consideration is accounting for the oscillator's nonviscous dissipation. This dissipation is usually a slowly varying function of frequency. Thus, because a high–Q oscillator can be used as a viscometer only in a narrow range of frequencies, the nonviscous dissipation can usually be adequately characterized by a single constant. A more elaborate characterization, e.g. the anelastic correction described in Appendix C, may be needed for a low–Q viscometer. The accuracy required of this characterization depends on the ratio of the nonviscous to viscous dissipations. Because this ratio is approximately proportional to the Q, it is crucial for a high–Q viscometer. The lower sensitivity to nonviscous dissipation is an advantage of low–Q viscometers.

Appendix C: Corrections for anelasticity of the torsion fiber

The assumption of an ideal torsion spring in Eqs.(8) and (9) is known to fail for real

materials. (Although not applicable here, one such failure is nonlinearity, for example, exceeding the yield stress.) In low–amplitude oscillators, the best known manifestation of nonideal behavior is internal friction. The general phenomenon is known as anelasticity, and a material's compliance $J(\omega)$ can be written as a complex function of frequency [11]

$$J(\omega) = J_1(\omega) - iJ_2(\omega) . \qquad (C1)$$

This representation is commonly used in polymer rheology [12], and it has also been applied to "harder" materials such as metals, where there have been only limited studies of $J(\omega)$. Several recent studies found no significant frequency dependence of the loss compliance $J_2(\omega)$ in Be–Cu torsion fibers [13,14] and in a steel flexure pivot [15]. In contrast, there are studies [16,17] of pure metals where $J_2(\omega)$ was found to be frequency–dependent, generally decreasing with frequency.

We found three indications for anelasticity in the oscillating screen's torsion fiber. The first, seen at low frequencies, was a phase lag approximately independent of frequency (~0.2° at room temperature). The second, seen in the same frequency range, was a frequency dependence of the magnitude of the spring constant (~1% decrease upon going from 0.1 to 0.001 Hz at room temperature). The third indication was a slow relaxation of the oscillator's position following a step change in the applied force. The amplitude of this "elastic after–effect" was about 1% of the rapid initial change of the position, and its relaxation could be approximately described by an exponential with a time constant of about 400 s.

We initially considered other mechanisms for these effects. However, the elastic after–effect was observed with an applied magnetic as well as an electrostatic force, indicating behavior intrinsic to the oscillator. Also, a search at low frequencies for a subtle frequency–dependent error in the electronic instrumentation found nothing significant. We thus incorporated anelasticity into the description of the oscillator because it had a significant though small effect on the data. The final consistency achieved, both in a dispersion analysis of the anelasticity as well as in the viscosity data, justified this incorporation.

Anelasticity was added to the model of the oscillating screen by generalizing Eq.(8) for the transfer function to

$$H(\omega)^{-1} = k_0[(1-\Omega^2) + i\Omega^2(\rho/\rho_s)B(R/\delta) + k^*] , \qquad (C2)$$

where the spring constant k_θ was generalized to a complex function of frequency. This was done, consistent with Eq.(C1), by modifying the spring constant k_θ with a complex

perturbation k^* according to

$$k_\theta(\omega) \equiv k_0[1 + k^*] , \tag{C3}$$

$$\equiv k_0[1 + k_1(\omega) + ik_2(\omega)] . \tag{C4}$$

At the vacuum resonance frequency, the real part of the spring constant was defined to be

$$k_0 \equiv \mathrm{Re}[k_\theta(\omega_0)] . \tag{C5}$$

This definition and the measurement of the oscillator's Q in vacuum fix the value of the anelastic correction at ω_0:

$$k^*(\omega_0) \equiv 0 + iQ^{-1} . \tag{C6}$$

In the absence of viscous damping the frequency–dependent part of the spring constant k^* was obtained from the measured transfer function according to

$$k^*(\omega) = [H(\omega)/k_{tr}]^{-1} - (1-\Omega^2) . \tag{C7}$$

Fig. 9b shows a plot of the loss factor $k_2(\omega)$. We described its frequency dependence by a function linear in $\log(\omega)$, namely

$$k_2(\omega) \equiv A_2 + B_2 \log_{10}(\omega/\omega_0) . \tag{C8}$$

By making use of a Kramers–Kronig relation, the function $k_1(\omega)$ can be approximately described with no additional parameters according to:

$$k_1(\omega) = \frac{-2\ln(10)}{\pi}\left[A_2 \log_{10}(\omega/\omega_0) + \frac{B_2}{2} - [\log_{10}(\omega/\omega_0)]^2\right] . \tag{C9}$$

Fig. 9a compares Eq.(C9) with the values of $k_1(\omega)$ derived from the transfer function by Eq.(C7). The agreement was sensitive to the value chosen for the transducer coefficient k_{tr} and therefore determined the value of k_{tr}. In practice we used an initial value of k_{tr} determined from $H(\omega)$ at 0.1 Hz and then adjusted it slightly to force agreement with Eq.(C6), namely, $k_2(\omega_0) \equiv 0$. The values of $k_2(\omega)$ were insensitive to this adjustment of k_{tr}.

In general we required the values of the anelastic parameters A_2 and B_2 at all temperatures used in the viscosity measurements. For $A_2(T)$, we used measurements of the oscillator's Q in vacuum. For $B_2(T)$, we relied on low–frequency measurements made in vacuum at 23° C and in low–density CO_2 at higher temperatures. (The vacuum measurements were made before the anelastic effect was understood, and thus low–frequency measurements in vacuum were made only near room temperature. Future oscillators will be characterized in vacuum at low frequencies at other temperatures.) Fig. 10 summarizes the results for $A_2(T)$ and $B_2(T)$.

We incorporated the anelastic correction into our viscosity measurements in two ways. First, we used Eq.(C2) with $k^*(\omega)$ given by Eqs.(C8) and (C9). Second, we made a

small correction to the nominal transducer coefficient k'_{tr}, which was defined by $H(\omega)$ at 0.1 Hz. This value was then adjusted for consistency with Eq.(C9) according to

$$k_{tr} = \frac{k'_{tr}}{[1 - k_1(0.1\ \mathrm{Hz})]} . \qquad \text{(C10)}$$

We emphasize that the parameters A_2 and B_2 used in the anelastic corrections were determined entirely by measurements made at low frequency. The importance of the anelastic correction was greatest in the measurements of CO_2 at low density, precisely where the existing viscosity data are the most accurate. Fig. 11 is the equivalent of Fig. 8 but without incorporating the anelastic correction. As expected the correction is ~1% in size.

Appendix D: Sensitivity to k_{tr} and electronic filter corrections

We estimated the importance of errors in the determination of the transducer factor k_{tr} by varying k_{tr} from its measured value. To achieve ±0.1% accuracy in the viscosity, k_{tr} must be determined to within about ±0.1%.

We also estimated the importance of errors in the determination of the time constants used to correct for the effects of four low–pass electronic filters. The effect of these corrections is indicated by Fig. 12, which is the same as Fig. 3 but without filter corrections. The three most important filters all had time constants of about 1.2 ms. To achieve ±0.1% accuracy in the viscosity, each of these time constants must be known to within about ±3%.

References

1. R.F. Berg and M.R. Moldover, Science Requirements Document, report to NASA Lewis Research Center (1992).

2. V. Vesovic, W.A. Wakeham, G.A. Olchowy, J.V. Sengers, J.T.R. Watson, and J. Millat, J. Phys. Chem. Ref. Data 19 763 (1990).

3. J. Kestin, S.T. Ro, and W.A. Wakeham, J. Chem. Phys. 56, 4114 (1972).

4. E. Vogel and L. Barkow, Z. Phys. Chemie, Leipzig 267, 1038 (1986).

5. J. Kestin, Ö. Korfali, and J.V. Sengers, Physica 100A, 335 (1980).

6. J. Kestin, W.H. Whitelaw, and T.F. Zien, Physica 30, 161 (1964).

7. H. Iwasaki and M. Takahashi, J. Chem. Phys. 74, 1930 (1981).

8. R.F. Berg and M.R. Moldover, J. Chem. Phys. 93, 1926 (1990).

9. G.G. Stokes, Mathematics and Physical Papers, Vol. III, p.11 (Cambridge University, London, 1922); R.G. Hussey and P. Vujacic, Phys. Fluids 10, 96 (1967); R.E. Williams and R.G. Hussey, Phys. Fluids 15, 2083 (1972).

10. R.F. Berg, unpublished.

11. A.S. Nowick and B.S. Berry, Anelastic Relaxation in Crystalline Solids (Academic Press, New York, 1972).

12. J.D. Ferry, Viscoelastic Properties of Polymers, 3rd ed. (Wiley, New York, 1980).

13. T.J. Quinn, C.C. Speake, and L.M. Brown, Phil. Mag. A 65, 261 (1992).

14. W.L. Tew, T.J. Quinn, R.S. Davis, and C.C. Speake, Bull. Am. Phys. Soc. 38, 946 (1993).

15. P.R. Saulson, R.T. Stebbins, F.D. Dumont, and S.E. Mock, preprint (1992).

16. J.L. Routbort and H.S. Sack, J. App. Phys. 37, 4803 (1966).

17. J. Woigard, M. Gerland, and A. Riviere, p. 293 in Internal Friction and Ultrasonic Attenuation in Solids, C.C. Smith ed. (Pergamon, New York, 1979).

Table 1: Approximate kinematic viscosity in $m^2 \cdot s^{-1}$ for representative densities of CO_2 near room temperature. The number in parentheses is the density in $kg \cdot m^{-3}$. Also shown is the minimum value for xenon.

Fluid:	$CO_2(3)$	$CO_2(30)$	$CO_2(300)$	$Xe(\rho_c)$
η/ρ:	5.1×10^{-6}	5.1×10^{-7}	7.6×10^{-8}	4.7×10^{-8}

Table 2: Viscosity values, in units of 10^{-5} Pa·s, used in the calibration tests. The data sources are indicated by letters as follows: (a)=[3], (b)=[5], (c)=[6]. Although our densities and temperatures were chosen to be close to those used in the referenced studies, small interpolations in density and temperature were necessary.

$\rho/kg \cdot m^{-3}$:	1.79	18.9	90.1	242.8	295.1
T(°C)					
25.6	1.495(a)				
31.6		1.530(b)	1.616(b)	2.054(b)	2.270(b)
31.6				2.028(c)	
34.6				2.046(c)	
40.6	1.568(a)			2.086(c)	
60.6	1.663(a)				

Table 3: Examples of the sensitivity to dissipation of two oscillators, defined as the magnitude of Eq.(A5).

frequency		Q = 0.1	Q = 10
"low"	$(\omega/\omega_0 = 1/2)$	0.99	0.067
resonance	$(\omega/\omega_0 = 1)$	1	1
"high"	$(\omega/\omega_0 = 2)$	0.99	0.067

Figures

1. The viscometer's sensitivity estimated from the model of a transversely oscillating cylinder with R≡13.8 μm. The two curves are for xenon at its critical density (1110 kg·m^{-3}) and for CO_2 at 295.1 kg·m^{-3}.

2. The transfer function H(ω) measured in CO_2 at 1.79, 18.9, 90.1, and 295.1 kg·m^{-3}. The lowest density data were obtained at 25.6° C, and the remainder were acquired at 31.6° C. (a) The magnitude of H. (b) The phase of H.

3. The hydrodynamic geometry function B(R/δ) calculated using Eq.(13) from the transfer function data shown in Fig. 2. The reference length is R≡13.8 μm, the viscosity values are from Kestin, Korfali, and Sengers [5], and the points are averaged in groups of 10. The curves are calculated from the cylinder model. (a) The function $(R/\delta)^2|B|$ is plotted to reduce the strong dependence on R/δ. (b) The phase of B.

4. The ratio $|B/B_c|$ is plotted to ease examination of the results of Fig. 3. Small differences exist between data sets at high frequencies, especially above 15 Hz. There is also a frequency–independent offset between the data at 90.1 and at 295.1 kg·m^{-3}. This offset is comparable to differences between viscosity values reported from different investigations at this density.

5. The function B/B_c obtained from the results of Fig. 3 after reducing the viscosity value from the data at 295.1 kg·m^{-3} by 1.0%. Only data in the frequency range 1–10 Hz are plotted. Because the points fall on a single smooth curve, they are consistent with the use of hydrodynamic similarity. The pronounced deviations from the ideal cylinder calculation B_c at low frequency are to be expected: the penetration depth is half the distance between screen wires at R/δ=0.033. (a) The magnitude of B/B_c. (b) The phase of B/B_c.

6. The function B/B_c obtained by varying the temperature at 242.8 kg·m^{-3}. For consistency in this comparison we used only data from Kestin, Whitelaw, and Zien [6]. Over the range $0.2 < R/\delta < 0.3$ the traces of $|B/B_c|$ obtained from the 31.6 and 40.6° C data are consistent to within a viscosity error of ±0.1%. The viscosity changes by 2.9% between these two temperatures. The trace from the 34.6° C data is significantly higher over the same range in R/δ, corresponding to a viscosity disagreement of as much as –0.2%.

7. The oscillator's transfer function H(ω) measured in CO_2 at 1.79 kg·m^{-3} at 25.6, 40.6, and 60.6° C. Although, the resulting variation in the viscosity (11%) was less than that resulting from varying the density, the most accurate data sets available are for viscosity vs. temperature at low density. (a) The magnitude of H. (b) The phase of H.

8. The hydrodynamic geometry function B(R/δ). The agreement is excellent up to

about R/δ=0.028 or about 12 Hz. At ±0.1%, the corresponding error in viscosity is consistent with the data of Kestin, Ro, and Wakeham [3] to within their stated accuracy. Thus, the oscillating's screen performance is consistent with the most accurate viscosity data available. (a) The magnitude of B/B_c. (b) The phase of B/B_c.

9. The anelastic contribution to the spring constant as defined by Eqs.(13–15), measured at 23° C. (a) The real part $k_1(\omega)$. The curve is calculated from Eq.(20) using parameters derived from the linear description of $k_2(\omega)$. (b) The imaginary part $k_2(\omega)$. The linear description of the data, Eq.(19), was forced to go through the vacuum measurement of Q^{-1}, indicated by the lower circle. Because the low–frequency measurements were made in a degraded vacuum, viscous drag increased the apparent value of k_2 at frequencies above 1 Hz. The associated increased value of Q^{-1} is indicated by the upper circle.

10. The measured temperature–dependent values of the anelastic parameters A_2 and B_2, used in Eqs.(19) and (20). (a) The values of A_2 were defined by the values of Q^1 measured in vacuum. The curve is an empirical description of the data. (b) The values of B_2 derived from plots such as Fig. 9b. The straight line is an empirical description of the data.

11. The influence of the anelastic corrections can be seen by omitting them from the analysis used to draw Fig. 8a.

12. The importance of the corrections for the four low–pass electronic filters can be seen by omitting them from the analysis used to draw Fig. 3.

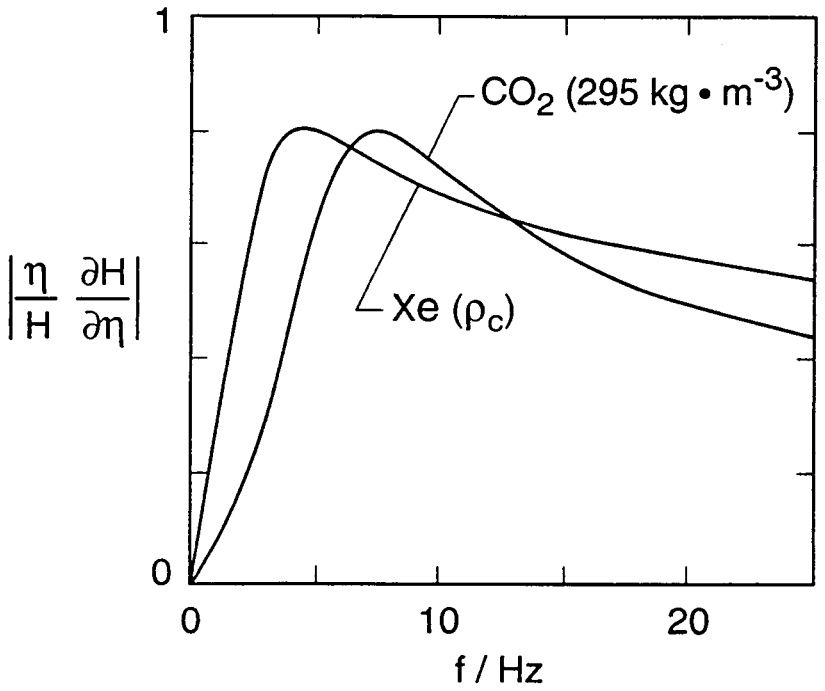
1
0
0
10
20
f / Hz
$\left|\frac{\eta}{H}\frac{\partial H}{\partial \eta}\right|$
CO_2 (295 kg • m^{-3})
Xe (ρ_c)

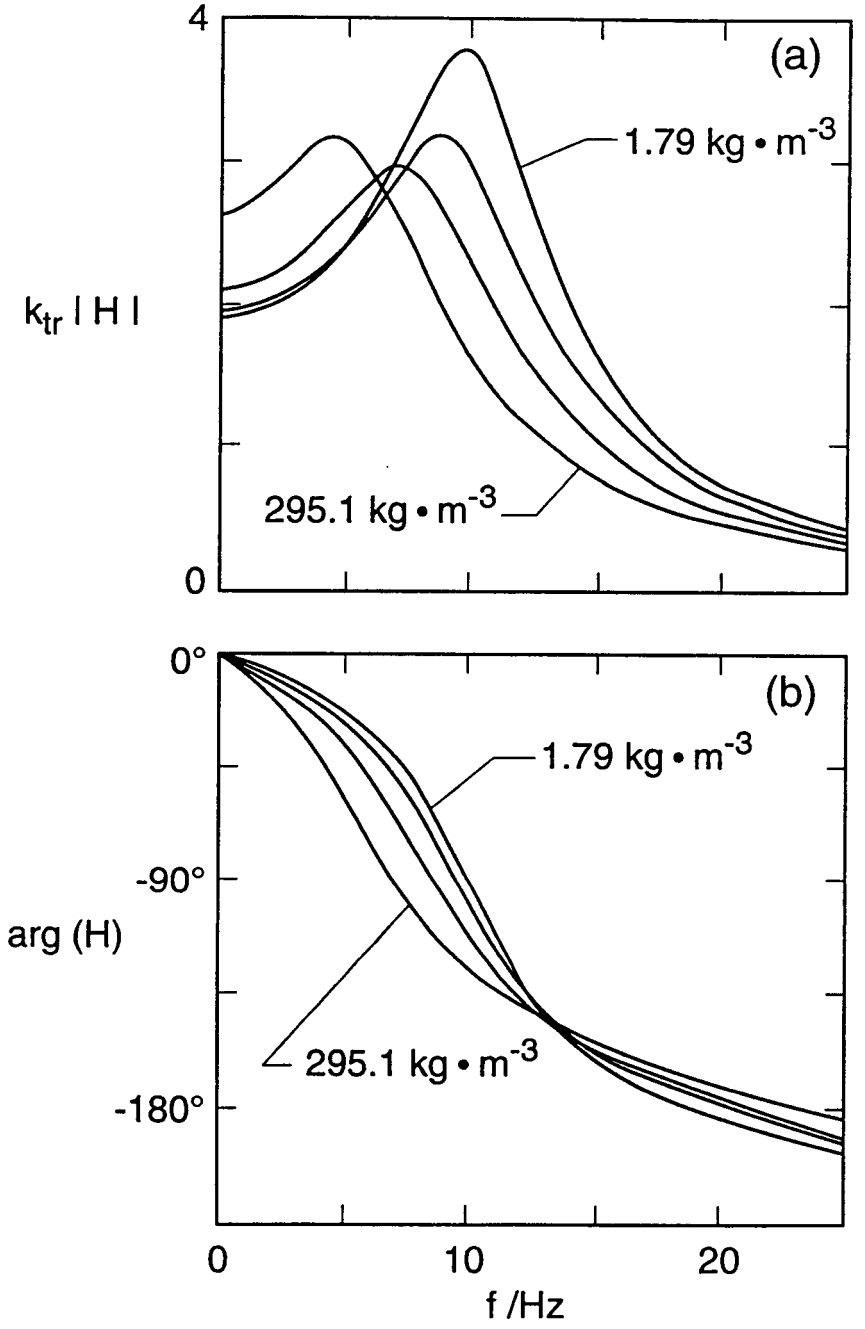
4
(a)
1.79 kg • m-3
ktr I H I
295.1 kg • m-3
0
0°
(b)
1.79 kg • m-3
-90°
arg (H)
295.1 kg • m-3
-180°
0
10
20
f /Hz

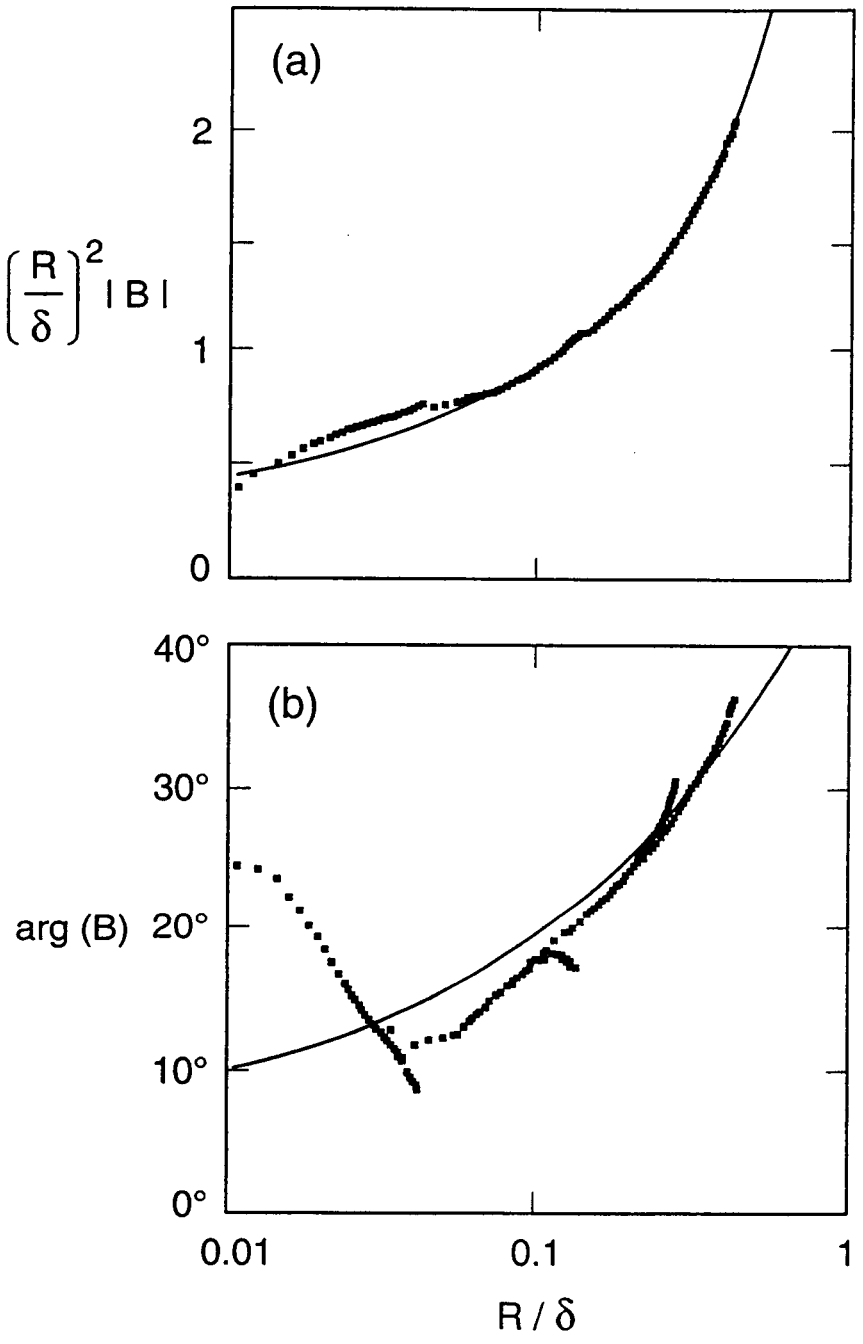
(a)
$\left(\frac{R}{\delta}\right)^2 |B|$
2
1
0
(b)
arg (B)
40°
30°
20°
10°
0°
0.01
0.1
1
R / δ

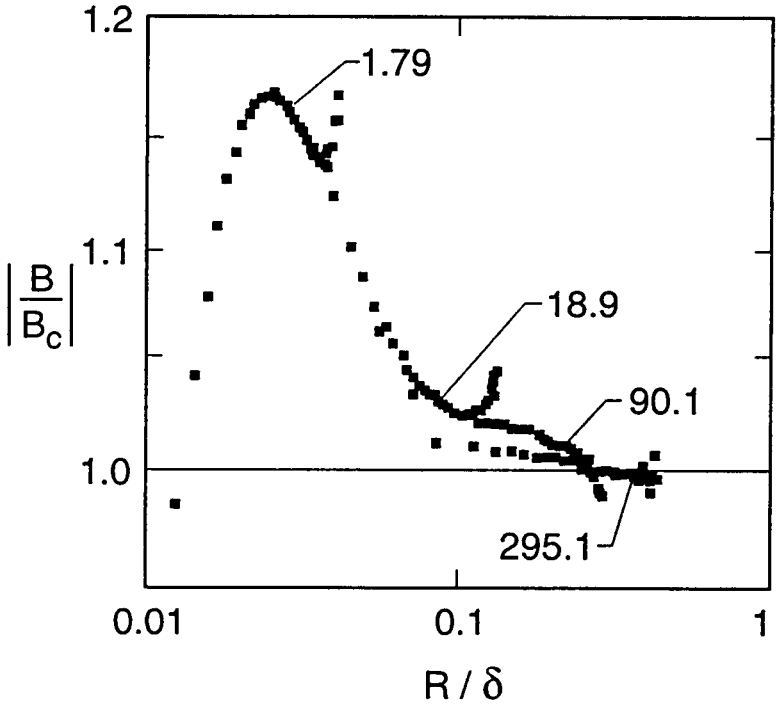
1.2
1.1
1.0
|B/Bc|
1.79
18.9
90.1
295.1
0.01
0.1
1
R / δ

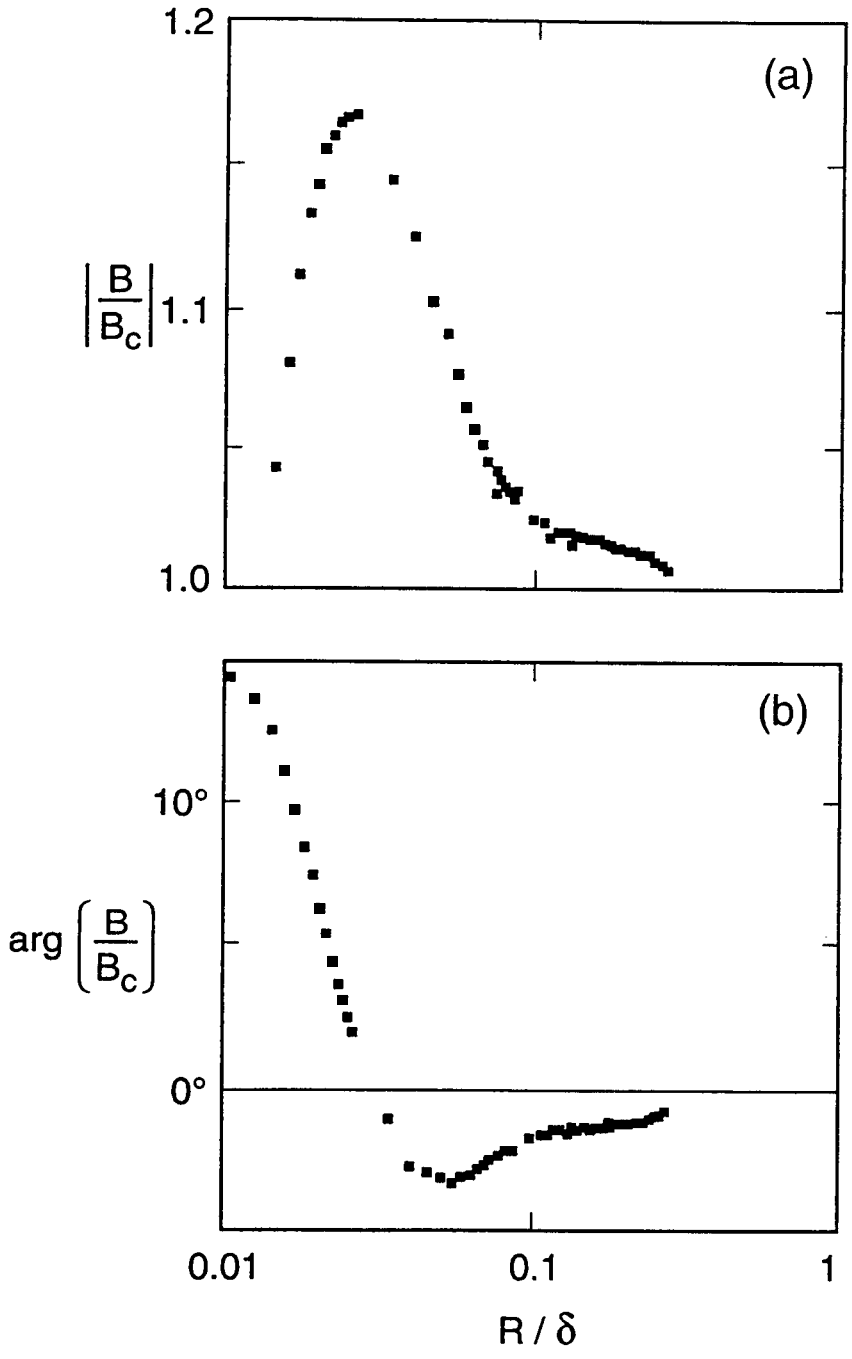
1.2
(a)
$\left|\frac{B}{B_c}\right|$ 1.1
1.0
(b)
10°
arg $\left(\frac{B}{B_c}\right)$
0°
0.01
0.1
1
R / δ

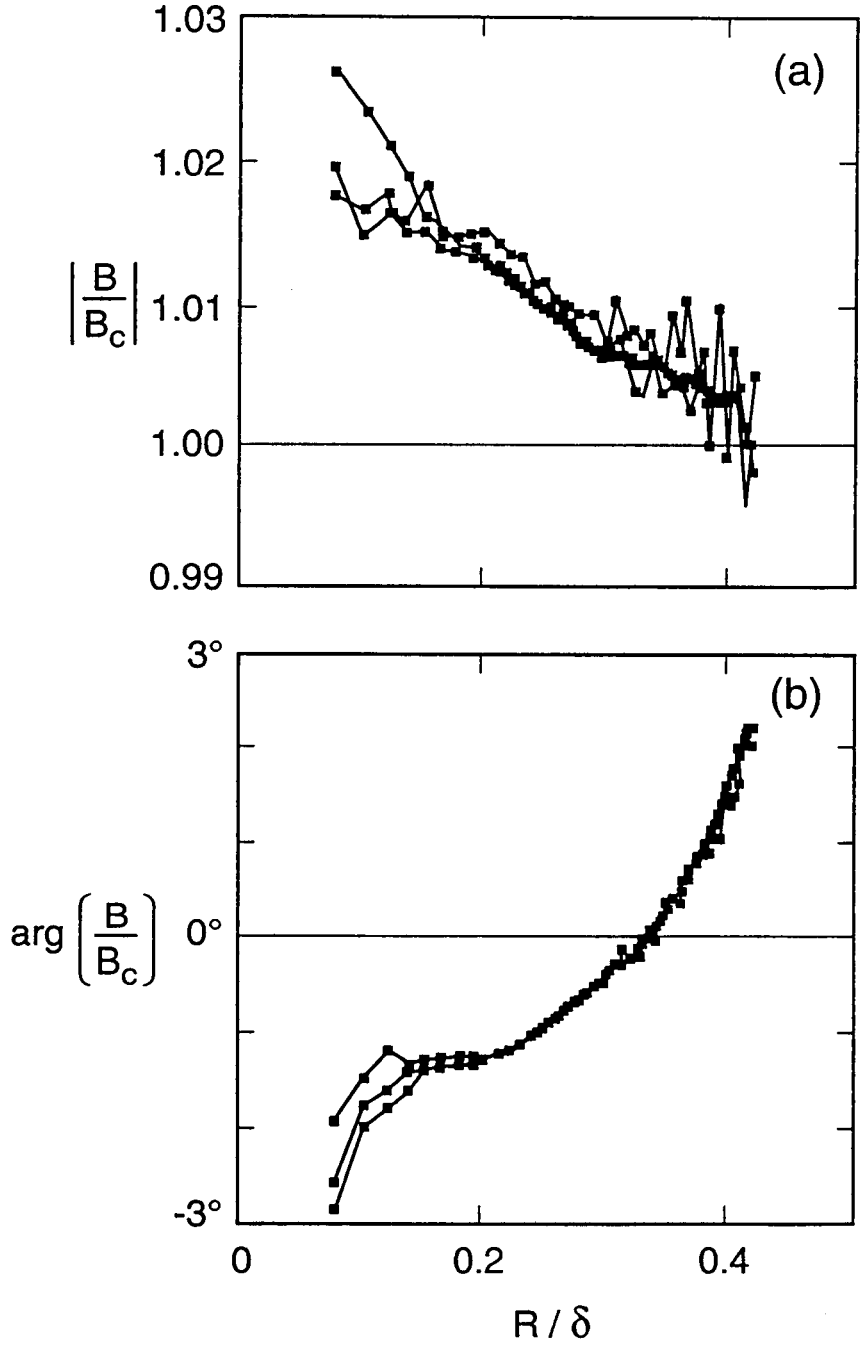
1.03
1.02
1.01
1.00
0.99
(a)
|B/Bc|
3°
0°
-3°
(b)
arg (B/Bc)
0
0.2
0.4
R / δ

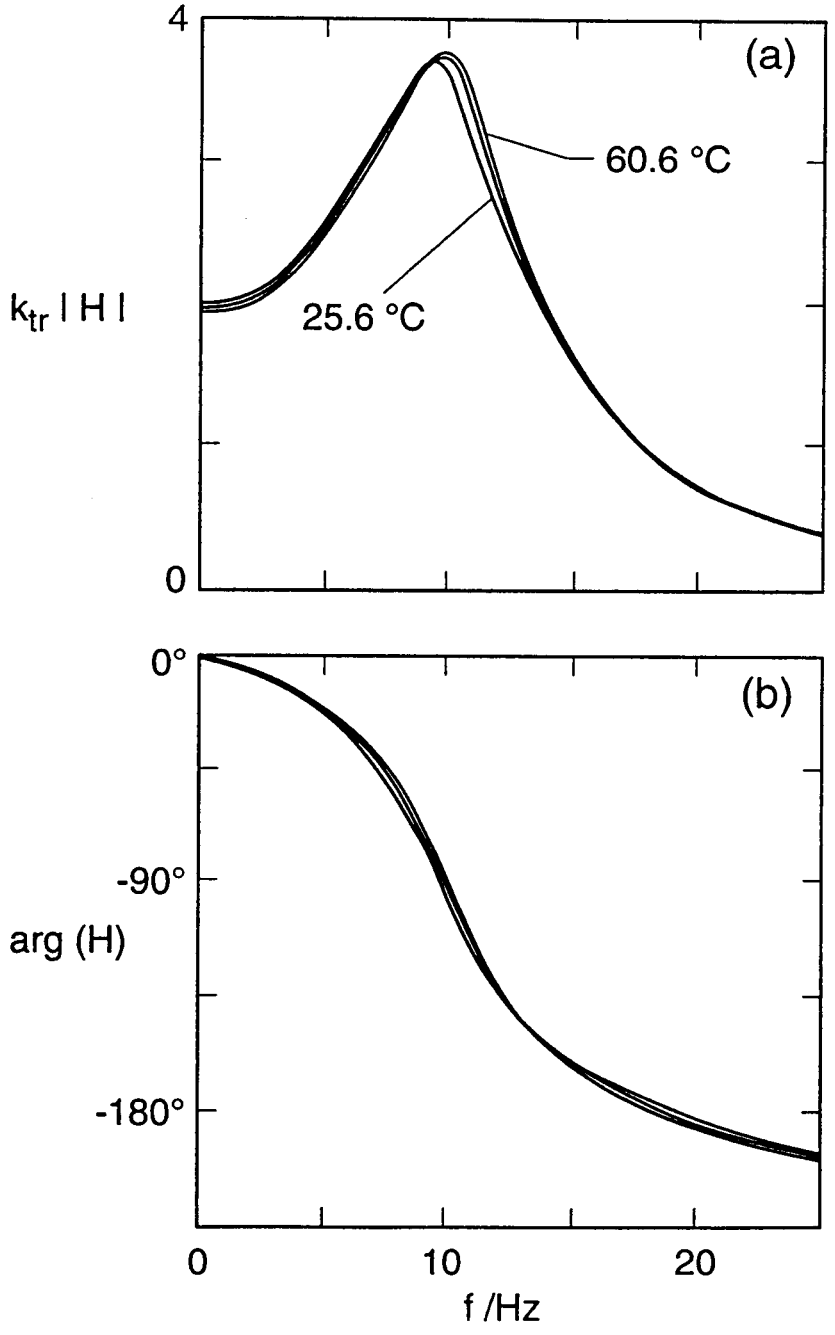
4
(a)
60.6 °C
25.6 °C
k_{tr} | H |
0
0°
(b)
-90°
arg (H)
-180°
0
10
20
f /Hz

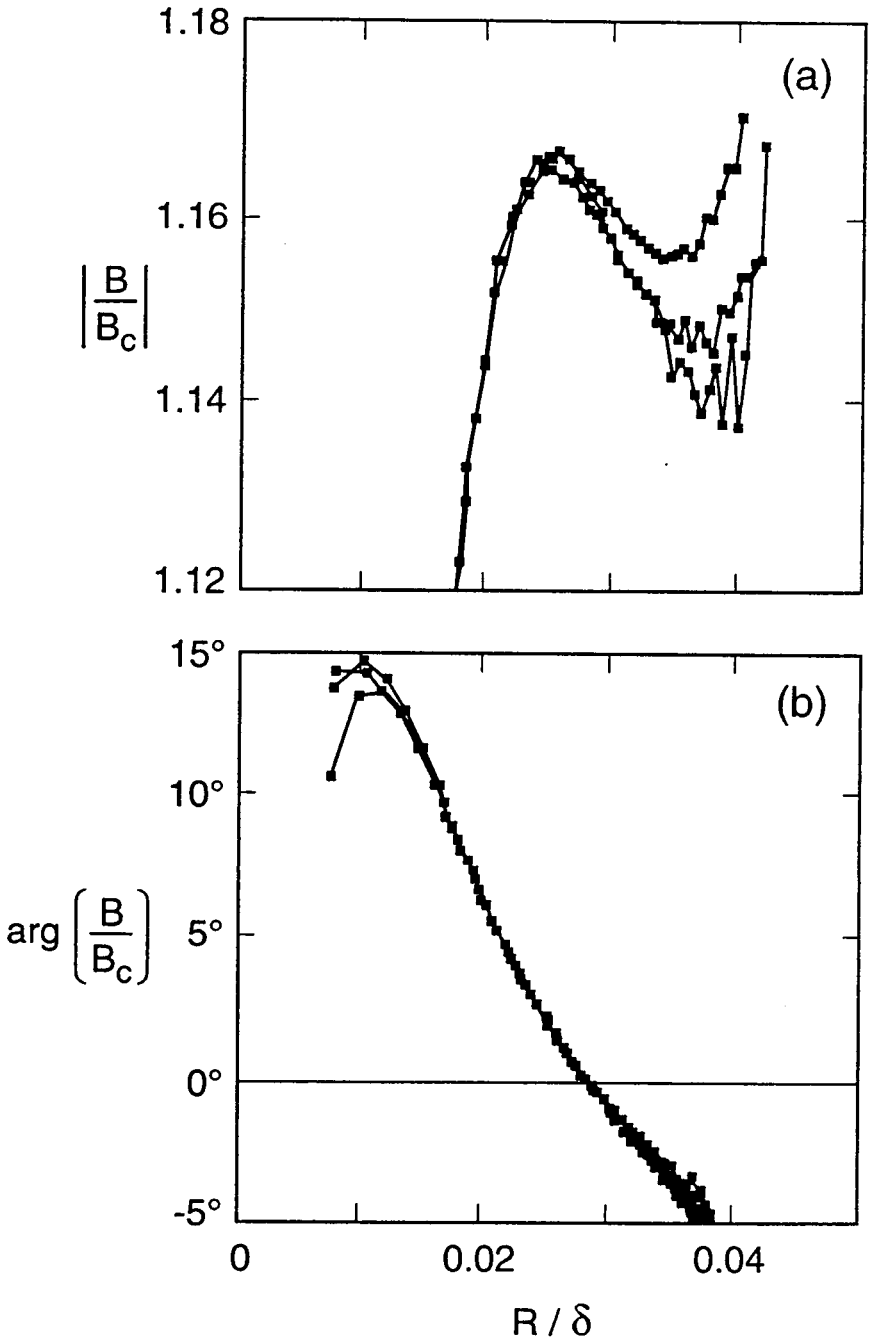
1.18
1.16
1.14
1.12
(a)
$\left|\frac{B}{B_c}\right|$
15°
10°
5°
0°
-5°
(b)
$\arg\left(\frac{B}{B_c}\right)$
0
0.02
0.04
R / δ

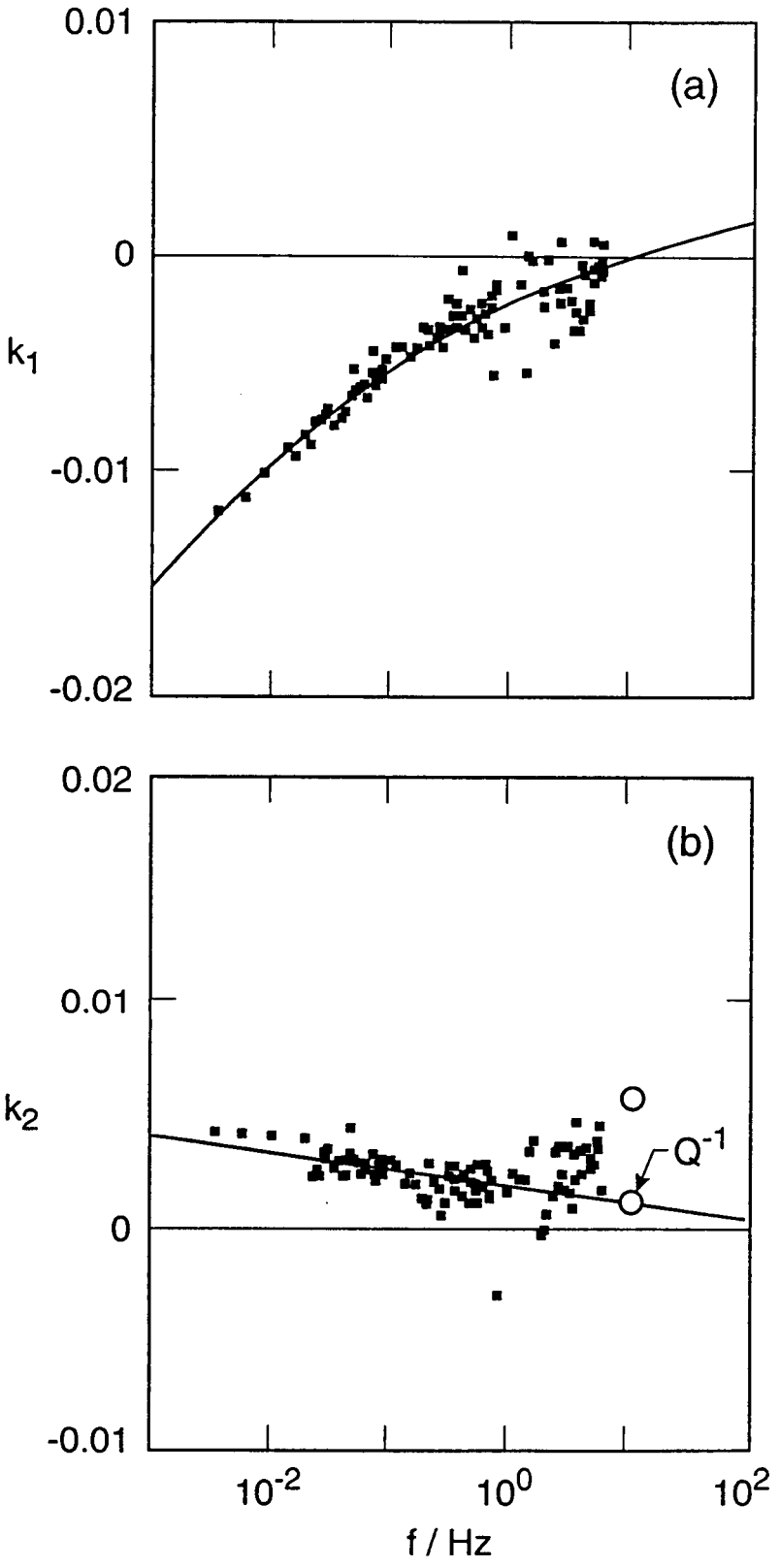
0.01
0
-0.01
-0.02
(a)
k_1
0.02
0.01
0
-0.01
(b)
k_2
O
Q^{-1}
10^{-2}
10^{0}
10^{2}
f / Hz

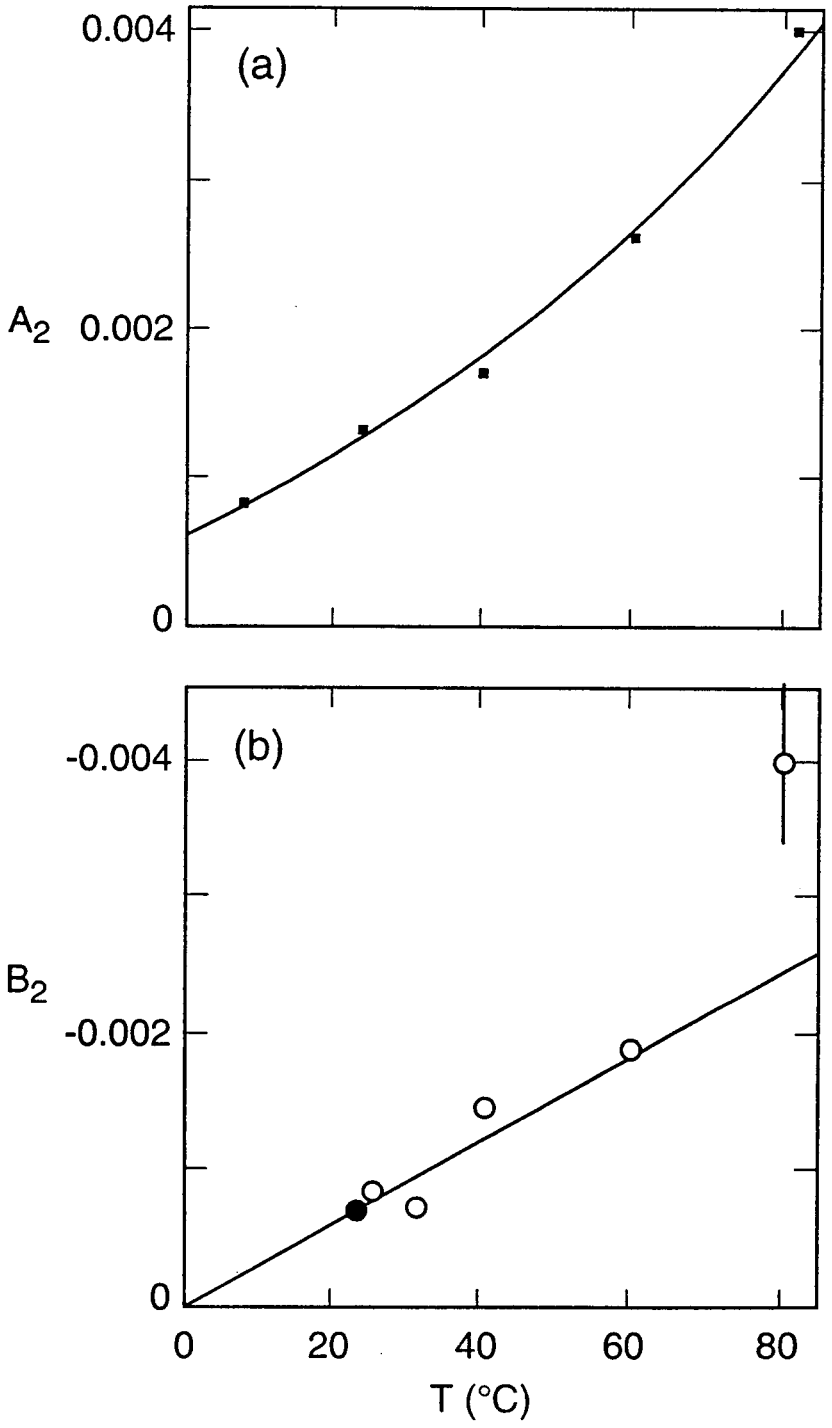
0.004
(a)
A_2
0.002
0
-0.004
(b)
B_2
-0.002
0
0
20
40
60
80
T (°C)

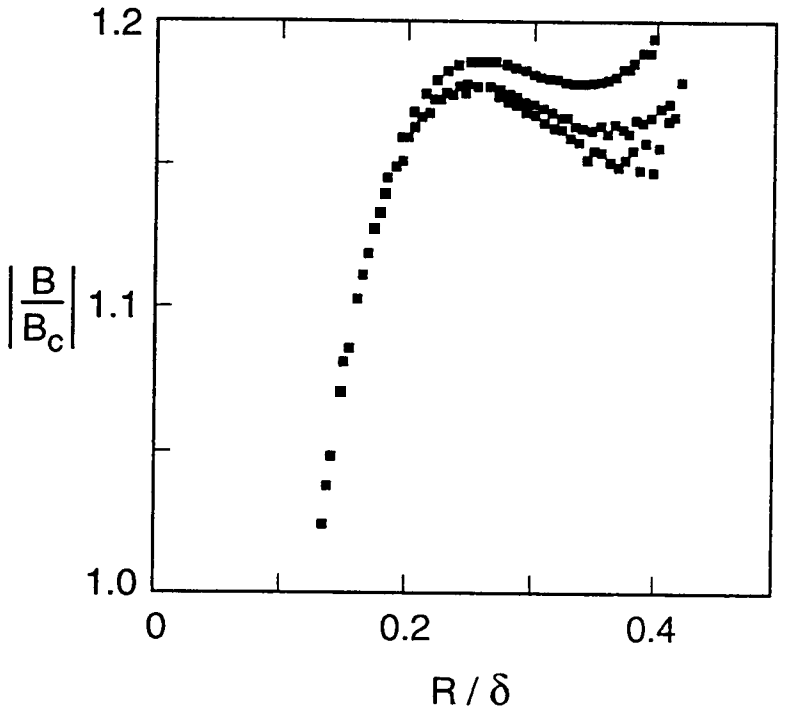
1.2
1.1
1.0
$\left|\frac{B}{B_c}\right|$
0
0.2
0.4
R / δ

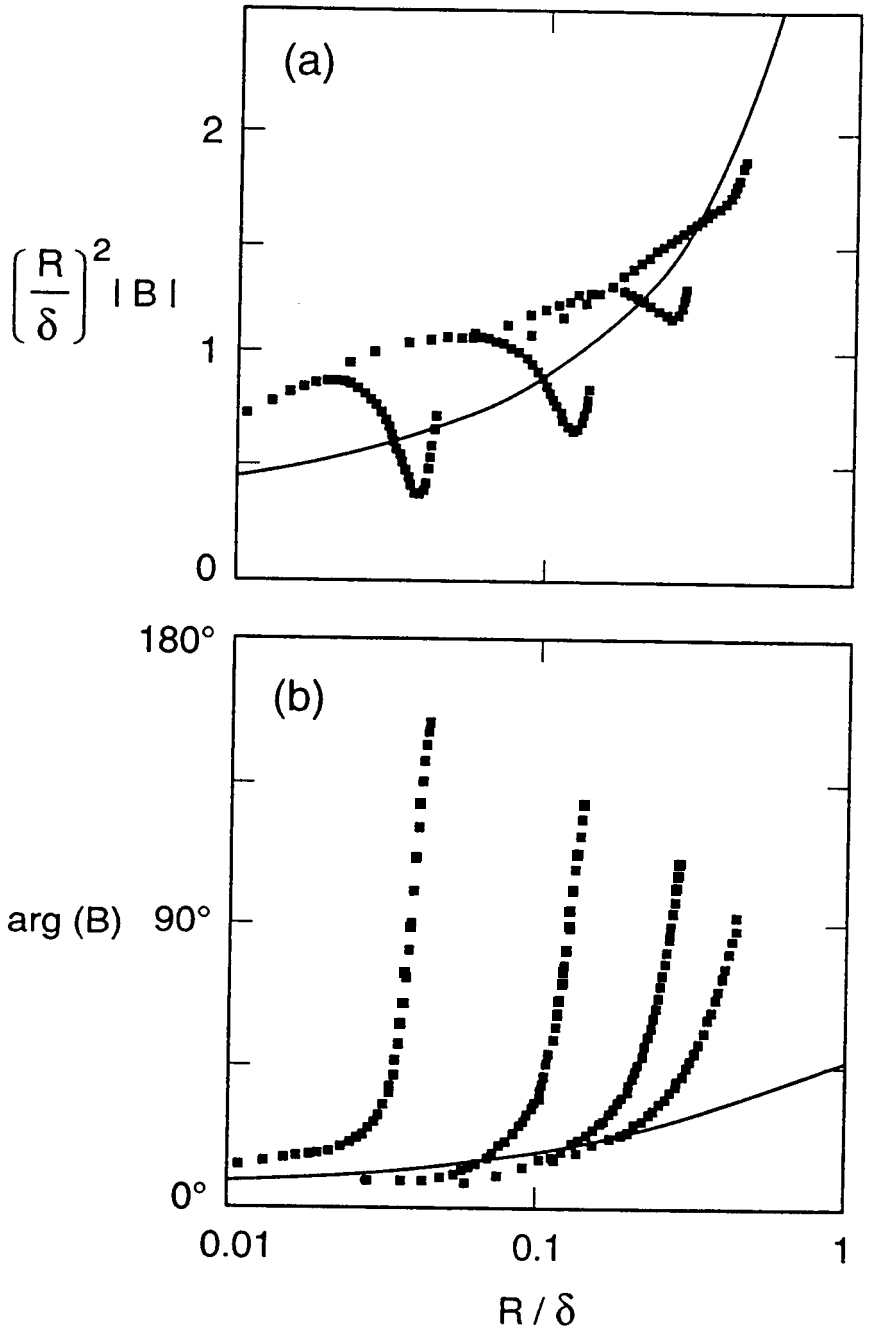
(a)
$\left(\frac{R}{\delta}\right)^2 |B|$
2
1
0
(b)
arg (B)
180°
90°
0°
0.01
0.1
1
R / δ